Received: 18 February 2019 | Revised: 21 March 2019 | Accepted: 25 March 2019

DOI: 10.1002/jsid.786

DISTINGUISHED PAPERS, BEST OF DISPLAY WEEK 2019

WILEY

OLED display incorporating organic photodiodes for fingerprint imaging

Taisuke Kamada | Ryo Hatsumi | Kazunori Watanabe | Susumu Kawashima | Masahiro Katayama | Hiroki Adachi | Tetsuji Ishitani | Koji Kusunoki | Daisuke Kubota | Shunpei Yamazaki

Semiconductor Energy Laboratory Co, Ltd, Atsugi-shi, Japan

Correspondence
Taisuke Kamada, Semiconductor Energy Laboratory Co, Ltd, 398 Hase, Atsugi-shi, Kanagawa, 243-0036, Japan.
Email: tk1344@sel.co.jp

Abstract

This paper introduces and demonstrates a display that incorporates an organic image sensor formed in the same pixel as organic light-emitting diodes through side-by-side patterning. The potential applications of this display include touch sensing, scanning, and fingerprint identification at any location on the entire display screen, without the necessity of an external module.

KEYWORDS

crystalline oxide semiconductor, OLED, OPD

1 | INTRODUCTION

Recent mobile terminals, ie, smartphones, have been incorporated with more versatile functions that extend beyond the norm of accessing information, as in the case of personal information exchange for digital payments. On this aspect, the protection of individual security via individual authentication functions, eg, fingerprint identification functions,[1] has been a growing necessity for mobile terminal applications, along with the reduction of the bezel size of these terminals. In fact, compact and thin displays with large screens, as well as bezel-less displays, have been developed and are currently in demand, due to the improved portability, convenience, and visibility they offer. On this note, products with display-to-terminal area ratios of over 90% are already available in the mobile terminal market.

On the one hand, many conventional modules used in fingerprint identification for personal authentication are placed outside the display region in the front of the terminals. However, such location is undesirable for the bezel-less display. On the other hand, the terminals including the modules on the rear and the side of the terminals can be found in the market. In addition, more recent fingerprint identification modules are placed behind the display modules.[2] In any of the above cases, the modules are mounted as separate components, resulting to design problem relative to compact and flexible displays.

Fingerprint identification modules come in various forms, ie, optical sensors,[3] whose mainstream for the identification are devices with Si-based active layers. Organic photodiode (OPD) using organic materials[4,5] is another form. OPD presents advantages over the Si-based sensor regarding area increase,[6] wavelength selectivity, cost reduction, and applicability to flexible devices, due mainly to the characteristics of the organic materials. Moreover, the device structure of an OPD is extremely similar to that of an organic light-emitting diode (OLED).[7] The OPD and the OLED consist of an active layer or a light-emitting layer between the hole- and electron-transport layers and between electrodes.

Recently, some reports on a device incorporating an OPD and an OLED have been provided.[8,9]

Focusing on the similarity between the OLED and OPD device structures, we fabricated a prototype display that incorporates an OPD in each pixel through side-by-side patterning, generally used for fabricating OLED displays. Herein, we investigate the validity of the OPD-incorporating panel for fingerprint identification at any location within the entire display region and for color scanning as well.

2 | PROTOTYPE DISPLAY PRINCIPLE

Figure 1 shows a schematic of the device structures of OLEDs and an OPD in a pixel of the prototype display. Each pixel of the fabricated display consists of four devices, ie, three red-green-blue (RGB) OLEDs and an OPD, and respective pixel circuits for driving the devices. In these devices, the hole-transport layers (HTLs), the light-emitting layers of the OLEDs, and the active layer of the OPD are separately deposited via side-by-side patterning. Moreover, injection layers, an electron-transport layer, and an upper semitransparent electrode are deposited with a common mask. The OLEDs have a top-emission structure to emit light to the counter substrate side, while the OPD is configured to detect light entering from the counter substrate side. The pixel circuits and reflective anodes, which are to be separately formed for the respective devices, can be simultaneously formed through the same backplane process. Thus, practically, with a simple change from a side-by-side patterning for the RGB devices to that for four devices, including the RGB devices and a sensor, the OLEDs and the OPD can be separately and easily formed in the entire display region. Compared with the structure where a photosensor is mounted as another module, this structure is advantageous in terms of design, and further, in overall process and cost, owing to the simple fabrication of the compact and flexible panel.

Prototype display imaging is performed where the OLEDs are taken as light source and the OPD detects the reflective light from the specimen object. Figure 2 provides the schematic cross-sectional view of the imaging process. Note that when imaging of the fingerprint is performed, light emitted from the OLED reflects off the finger on the counter substrate and is detected by the OPD. Fingerprint imaging is achieved by utilizing a difference in reflectance between the finger ridges and valleys. The fingerprint can be imaged monochromatically; color imaging can also be performed when light is sequentially emitted in RGB and reflected light of each color is detected by time division. For example, a

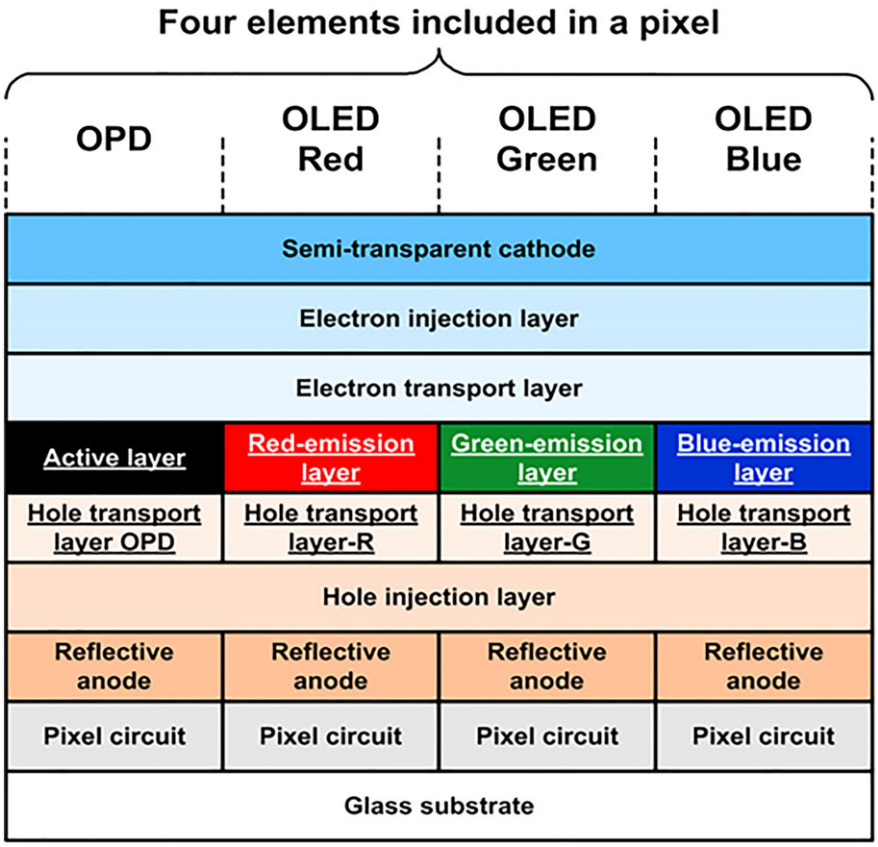

FIGURE 1 Structure of the devices included in a pixel. OLED, organic light-emitting diode; OPD, organic photodiode

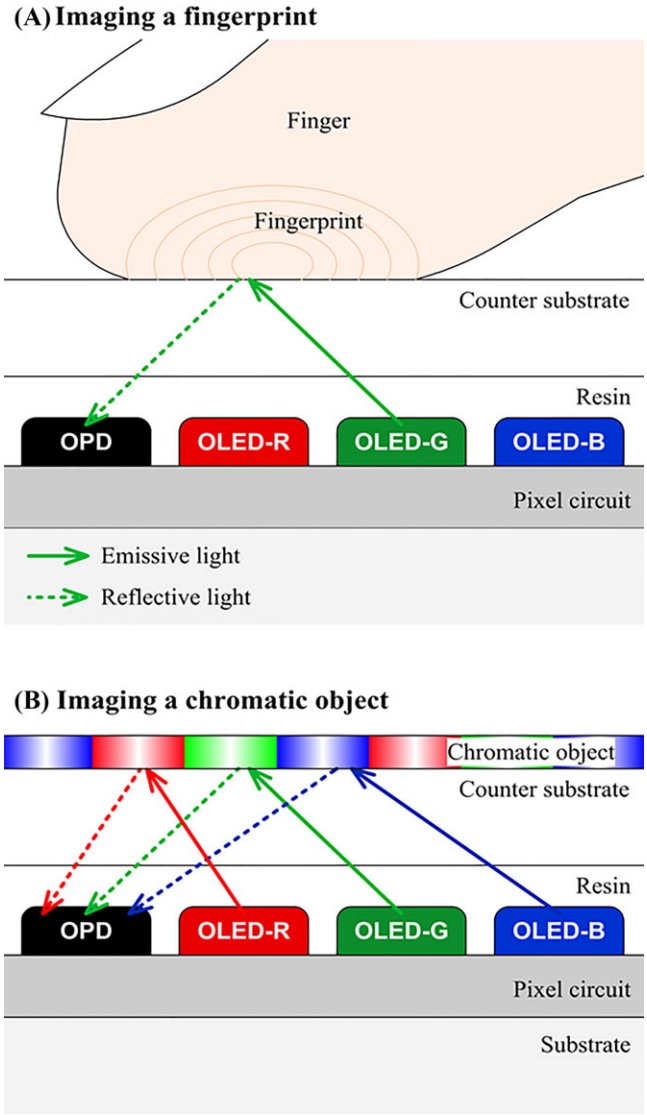

FIGURE 2 Detection by the OPD. OLED, organic light-emitting diode; OPD, organic photodiode

chromatic object placed on the counter substrate as in Figure 2B can be scanned in color. Furthermore, this method needs only photosensors with sensitivity to the entire visible light region and not individual photosensors for RGB, which is advantageous in increasing the resolution. In this manner, the OPD is incorporated in the panel through the side-by-side patterning, whereby the panel can be applied to a variety of uses.

3 | CHARACTERISTICS OF OPD FABRICATED IN THE PROTOTYPE DISPLAY

In the device structure of the OPD in the prototype panel, as in Figure 1, organic layers other than the active layer and the HTL are formed with the same thickness of the same materials as those in the OLEDs. Moreover, this OLED display employs a top-emission structure, including a semitransparent electrode in the upper portion to obtain a microcavity effect. In this case, the OPD, which partly shares the device structure with the OLEDs, is also affected by the microcavity effect. Therefore, this structure improves color purity and the like of the OLEDs but narrows the photosensitive wavelength range of the OPD. We fabricated four kinds of OPDs with different HTL thicknesses with 2 mm × 2 mm pixel size to investigate the wavelength dependence of sensitivity and the influence of the thickness of the HTL in the OPD used in the prototype panel. Figure 3 shows the spectral responsivity (SR) at an incident light intensity of 25 $\mu W/cm^2$ and the absorption spectrum of the active layer of the OPD.

From the figure, absorption by the active layer exists in the entire visible light region whereas it decreases in the red region. The actual SR of the OPD has a peak shift depending on its HTL thickness and, thus, needs to be adjusted appropriately to the wavelength region intended for the sensing. In the fabricated display, green light is emitted for fingerprint imaging. OPDs in the fabricated display employs a 40-nm-thick HTL, broadly covering the blue region and the red region as well as the green region in the middle, to enable both fingerprint and color imaging.

Figure 4 shows the relation between incident light intensity and photocurrent that flows when light of a 550-nm wavelength is incident on the OPD with a 40-nm HTL thickness presented in Figure 3. A linear relationship is observed between the incident light intensity and the photocurrent at applied voltages lower than or equal to −2 V. In particular, at −3 to −6 V, the voltage

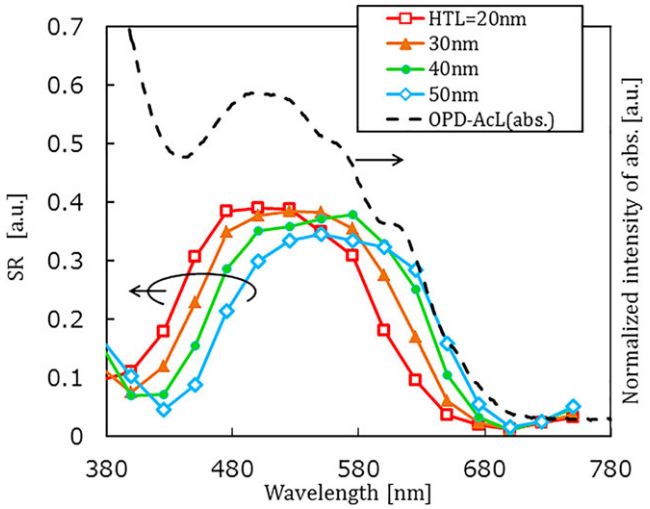

FIGURE 3 Relation between wavelength dependence of sensitivity and thickness of HTL. HTL, hole-transport layer; OPD, organic photodiode; SR, spectral responsivity

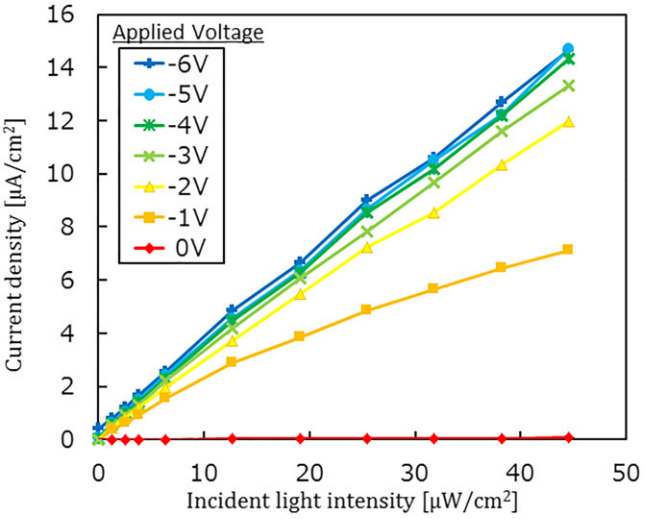

FIGURE 4 Relation between incident light intensity and photocurrent

dependence is small, that is, a saturation region is included. The dark currents at −3 and − 6 V were 1.15×10^{-8} and 3.91×10^{-7} A/cm^2, respectively. Image scanning requires an analog grayscale sensing, while color scanning requires detection sensitivity to a broad wavelength region. Figures 3 and 4 demonstrate that the OPD, which partly shares the device structure with the OLEDs, satisfies the above requirements and has no problem in operating as a photosensor.

4 | PROTOTYPE DISPLAY

4.1 | Structure of the prototype display

The backplane of the fabricated prototype display includes field effect transistors (FETs) as switching devices in which crystalline indium-gallium-zinc oxide (IGZO), an oxide semiconductor, is used as their active layers.[10–12] Figure 5 shows the classification of crystalline IGZO ceramics. We discovered c-axis–aligned crystal (CAAC)-IGZO[13] in 2009, nanocrystalline IGZO (nc-IGZO)[14] in 2013, and cloud-aligned crystal (CAC)-IGZO[15] in 2016. Recently, Waseda et al proposed that these IGZOs fall into a boundary region between a crystal phase[16–18] of single and polycrystals and an amorphous phase[19,20] that is completely amorphous and regards the boundary region as a novel crystalline region.[21]

FETs exploiting crystalline IGZO as their active layers exhibit an extremely low off-state current,[22] a feature enabling a global shutter image sensor,[23] as well as a number of reduced display rewriting operations in still-image display, leading to low-power driving (idling stop [IDS] driving).[24]

IDS driving extends a retention period of the image display by utilizing the low off-state current and reducing the number of rewriting operations; that is, it achieves low-frequency driving. Thus, it improves the signal-to-noise ratio (SNR) when combined with a sensor, ie, a touch sensor.[25,26] Normally, the panel's rewriting operation serves as noise to reduce the SNR of the sensor. However, in IDS driving, the rewriting operation of the panel can be stopped in image retention periods, thus, allowing sensing to be performed without the influence of the rewriting-based noise. By contrast, in the prototype panel, a single frame is divided into display and sensing periods; with IDS driving at the latter, image rewriting operation is not performed to reduce noise. Furthermore, during fingerprint identification and scanning, the OLEDs are used as light source; therefore, they need to retain constant luminance, which is attainable with the IDS driving. Therefore, with the IDS driving, the noise is reduced for a more favorable conduct of sensing.

From the above descriptions, fingerprint identification and scanning are performed using the OLEDs as light source and detection of reflected light from an object. Here, the SNR is expected to increase with higher OLED luminance. Thus, we employed a pixel circuit, which we call Pixel AI,[27] on the prototype panel for high-luminance light emission. With this circuit, the luminance can be selectively improved in sensing; for instance, when emitting only green light, the prototype display can have a maximum luminance of 2000 cd/cm^2.

Table 1 shows the specifications of a prototype display, in which the IDS driving, a global shutter method, and the function of Pixel AI, are used.

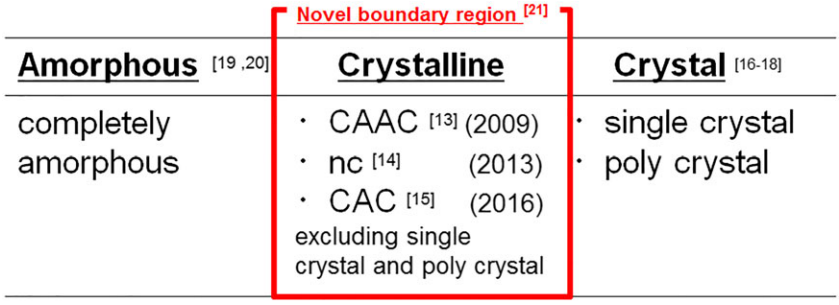

FIGURE 5 Classification of novel crystal structures or crystalline IGZO ceramics. CAAC, c-axis–aligned crystal; CAC, cloud-aligned crystal; IGZO, indium-gallium-zinc oxide; nc, nanocrystalline

TABLE 1 Display specifications

Screen diagonal	3.07 inches
Driving method	Active matrix
Resolution	360(H) × 540(V)
Pixel pitch	120 μm × 120 μm
Pixel density	212 ppi
Coloring method	Side-by-side patterning (RGB-OLED + OPD)
Emission type	Top emission
Gate driver	Integrated
Source driver	COG
Read out circuit	Analog output

Abbreviations: COG, Chip-on-Glass; OLED, organic light-emitting diode; OPD, organic photodiode; RGB, red-green-blue.

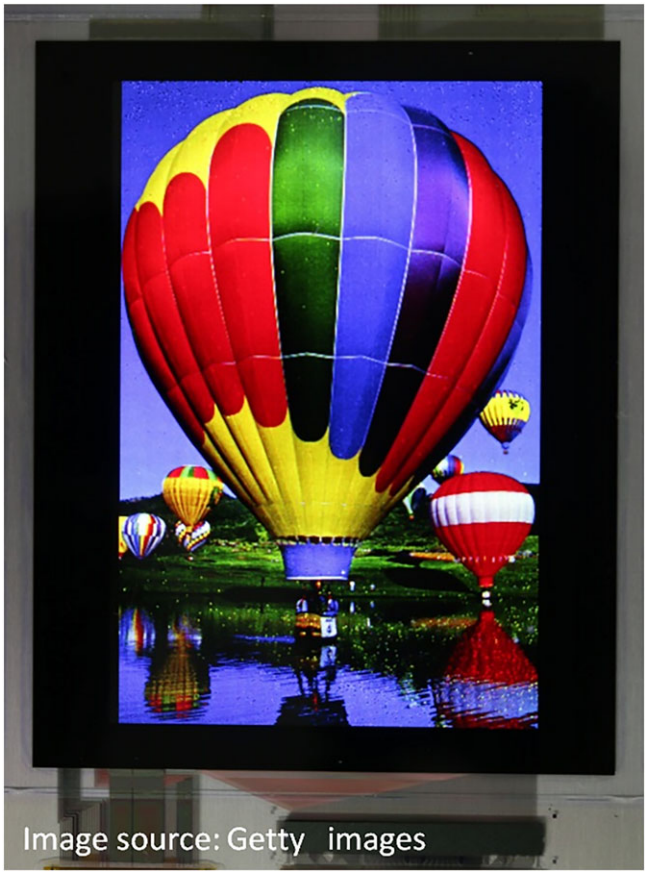

FIGURE 6 Displayed image

Figure 6 shows a photograph of the prototype display. Together with the OPD, our prototype panel can display an image favorably. Moreover, it advantageously facilitates formation of the flexible panel. In contrast, the structure currently available in the market, in which a Si-based Complementary Metal-Oxide-Semiconductor (Si-CMOS) sensor is mounted as a module different from the display panel, finds difficulty in creating a flexible region around the fingerprint identification module. Meanwhile, in the case where the OPD and OLEDs are formed within the same panel through side-by-side patterning as in our prototype panel, the entire display region can be made flexible by exactly the same method as that for a normal OLED panel. Figure 7 features a displayed still photograph of a prototype flexible panel.

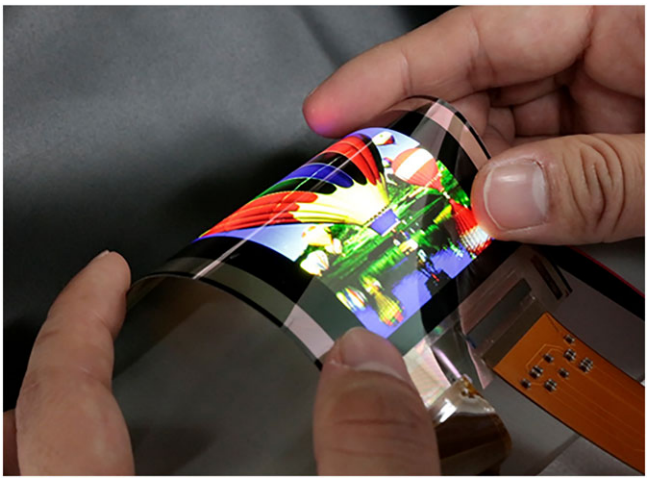

FIGURE 7 Still-image display on flexible display

4.2 | Imaging optical system

Figure 8 shows a schematic cross-sectional view of a pixel portion of the fabricated panel.

As explained with Figure 2, the prototype panel performs an imaging operation to allow light emissions from the OLED to be reflected by an object over the pixel and then detected by the OPD. Nonetheless, the process often generates stray light, which is emitted by the OLED but does not exit to the above and instead, travels inside the panel. Part of such light may directly enter the OPD without being reflected by the imaging object, as indicated by the dotted lines in Figure 8, and become noise to the imaging operation, thereby causing reduction in SNR. For this reason, a light-shielding layer is provided on both the circuit and the counter substrates to block the path of stray light and suppress noise generation in the prototype panel.

We compared the influence of stray light, with and without the light-shielding layer on both substrates, to examine the effect of the light-shielding layer. We allowed only a green pixel to emit light as light source, without placing anything on the panel, while we measured the light intensity detected by the OPDs positioned around the pixel. Here, as no object generating reflected

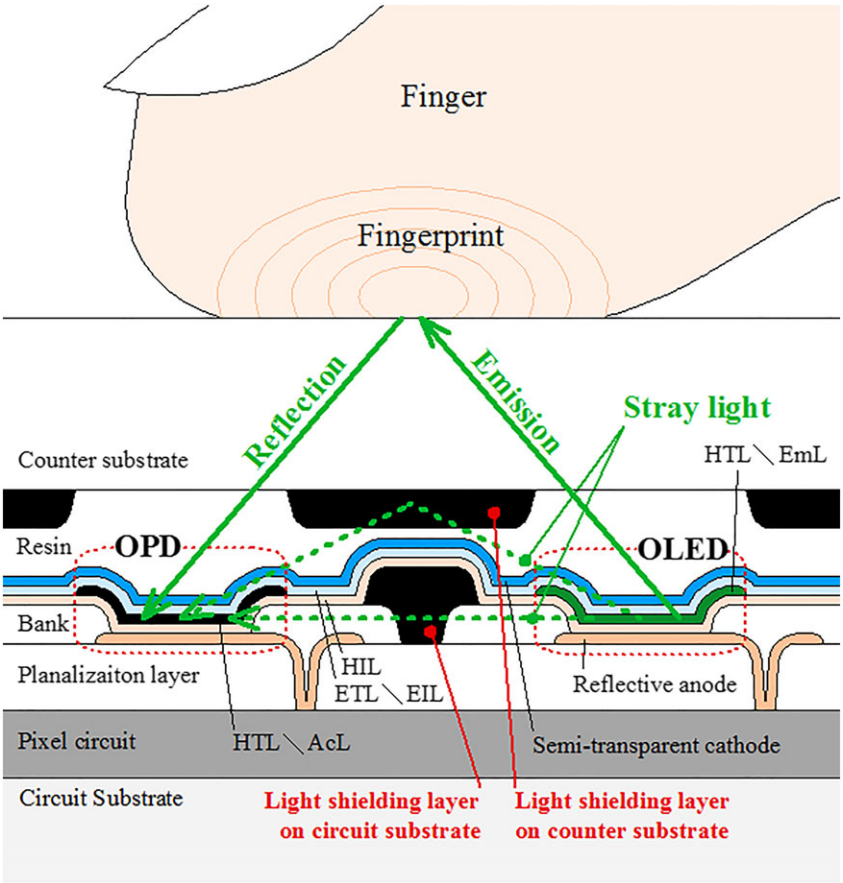

FIGURE 8 Schematic imaging optical system. EIL, electron-injection layer; ETL, electron-transport layer; HIL, hole-injection layer; HTL, hole-transport layer; OLED, organic light-emitting diode; OPD, organic photodiode

light, which becomes a signal, was put on the panel, the results shown in Figure 9 correspond to only detected noise component, including stray light generated from the light emission by the OLED. The Z axis represents the detected light intensity, and the X and Y axes represent the pixel address. To focus on only the influence of stray light from the OLED serving as a light source, we treated the detected light intensity shown in Figure 9, as the difference between the intensity detected in advance with the entire panel not emitting light, and the intensity detected with only the one pixel emitting light. In addition, we normalized the intensity with the measured peak intensity obtained, where the light-shielding layer was not provided.

Based on Figure 9, light was detected by OPDs around the light emission pixel regardless of the existence of the light-shielding layer. However, the maximum value of the intensity decreased by less than half by the provision of the layer. The effect of the shielding layer extended to the region several pixels away from the light emission pixel. When the layer was not provided, the intensity was high in 4×4 pixel region around the light emission pixel; on the contrary, after the layer was provided, the increased intensity area was limited to the region of 2×2 pixels. Thus, the light-shielding layer suppresses an increase in intensity and the spread of noise due to stray light and accordingly contributes to an improvement in SNR.

For a clear object image, each OPD was required to capture an image of the area directly over itself. The image became more blurry as the overlap of the image-capturing range between the OPDs of adjacent pixel addresses widened. To obtain a clear image with our prototype panel, we limited the image-capturing range of the OPD by adjusting openings in the light-shielding layer over the OPD and the OLED and the thickness of the counter substrate.

The image-capturing range of each OPD varied depending on the thickness of the counter substrate and the size of the openings. Subsequently, we examined the effects of the parameters on the image-capturing range. Figure 10 shows a schematic of the imaging optical system, including the opening in the light-shielding layer, where S is the image-capturing range of an OPD, L is the thickness of the counter substrate, p is the diameter of the opening in the light-shielding layer, l is the distance between the opening in the light-shielding layer and the OPD, and s is the OPD width.

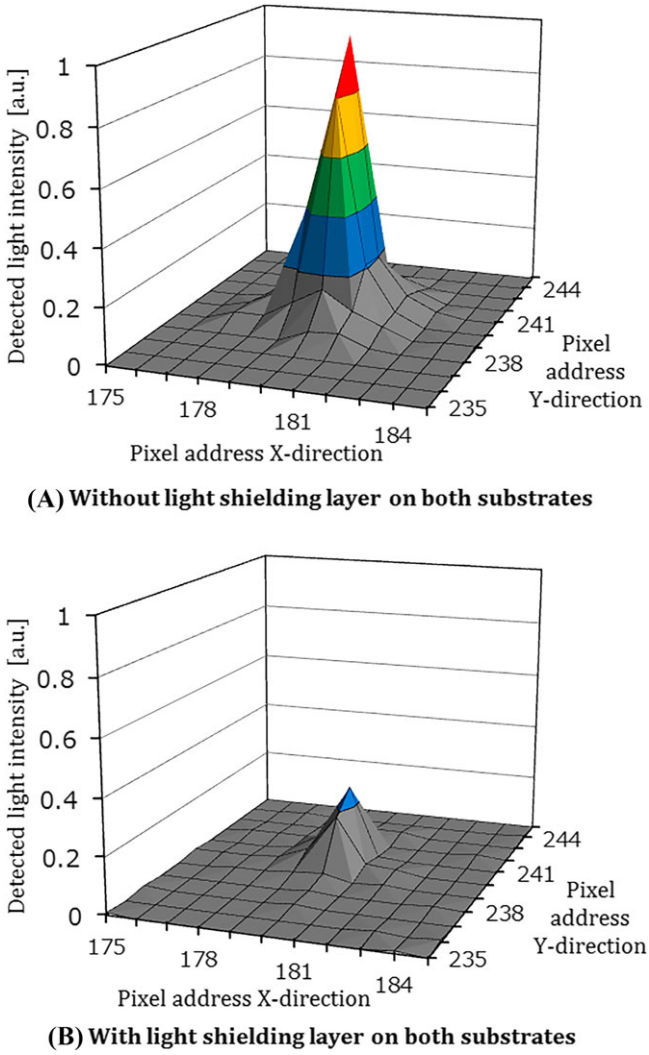

FIGURE 9 Comparison on the influence of stray light (A) without and (B) with light-shielding layer on both substrates

From the Figure 10, S, the image-capturing range of on OPD, is expressed as follows:

$$S = p + 2L\tan\theta_2. \tag{1}$$

θ_2 satisfies the following relation:

$$\sin\theta_2 = \frac{n_1}{n_2}\sin\theta_1 = \frac{n_1}{n_2}\frac{\frac{p+s}{2}}{\left[\left(\frac{p+s}{2}\right)^2 + l^2\right]^{\frac{1}{2}}}, \tag{2}$$

where n_1 and n_2 are the refractive indices of the adhesive resin and the counter substrate, respectively. From (1) and (2), S can be expressed as follows.

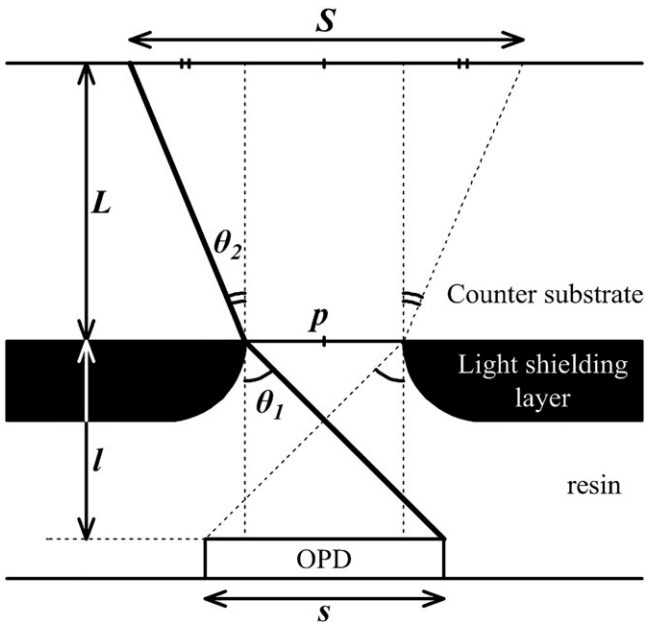

FIGURE 10 Schematic imaging optical system

$$S = p + L(p+s)\left\{\left(\frac{n_2}{n_1}\right)^2 l^2 + \left[\left(\frac{n_2}{n_1}\right)^2 - 1\right]\left(\frac{p+s}{2}\right)^2\right\}^{-\frac{1}{2}} \tag{3}$$

For the flexible display, in which case the refractive index of the sealing resin can be considered to be substantially equal to that of the substrate, we used resin film as the circuit and counter substrates. Applying $n_1 = n_2$ to (3) yields

$$S = p + \frac{L}{l}(p+s). \tag{4}$$

Figure 11 illustrates the S calculated with (4).

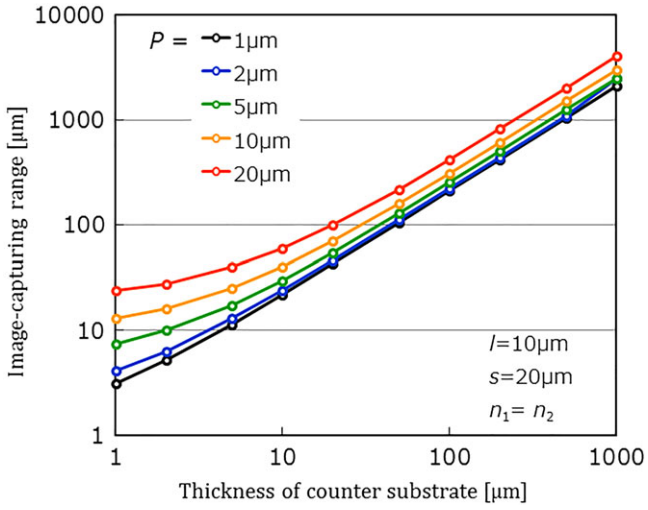

FIGURE 11 Relation between the diameter of the opening, the thickness of the counter substrate, and the image-capturing range

The smaller diameter p of the opening and the smaller thickness L of the counter substrate make the smaller image-capturing range. Given this setting, S can be controlled by p and L. A similar result can be obtained by increasing l and decreasing s in (4).

Figure 12 compares the image-capturing resolutions of the prototype panels with varying counter substrate thicknesses and with and without the light-shielding layer. For the image capturing, a reflective plate with a total light reflectance of 80% relative to the 550-nm wavelength, on which black lines having a width of 0.12 mm and a total reflectance of 5% were printed at 0.72-mm pitch, was placed on the panel. Specifically, the compared panels were designed to have 19, 8, and 21 μm of P, l, and s, respectively. Enlarged captured images are shown in Figure 12A, and the horizontal profiles extracted from the captured images are shown in Figure 12B, wherein the intensity was normalized with those of a low-reflectance black plate image captured in advance and a white background region.

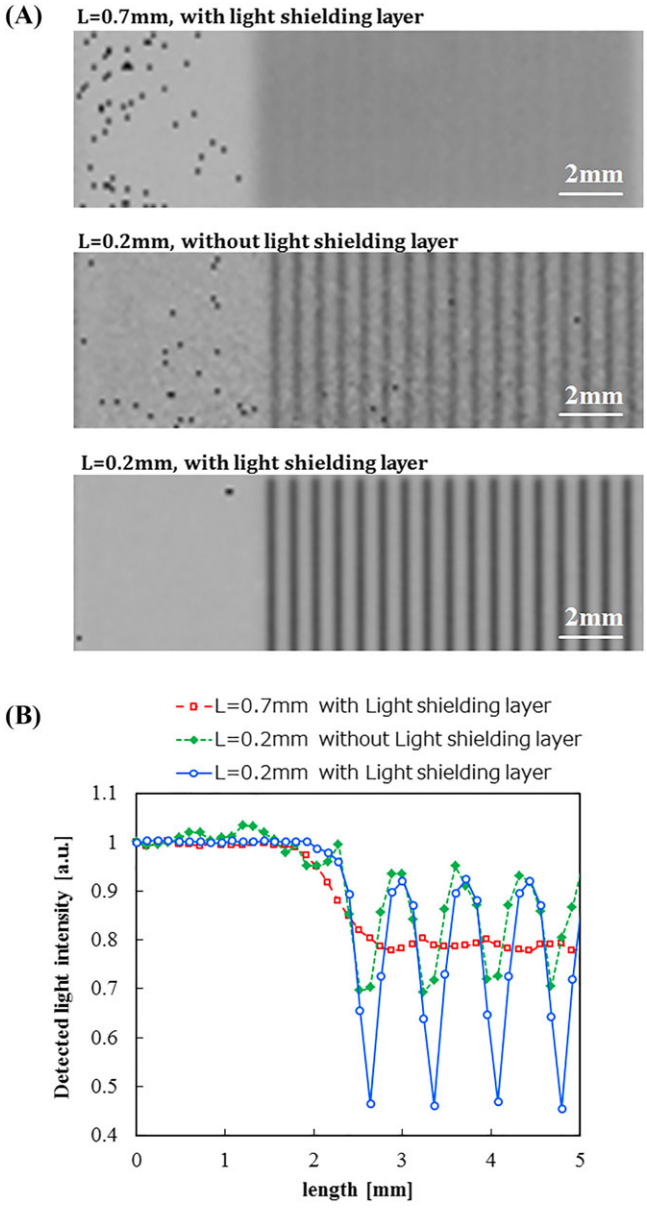

FIGURE 12 Comparison of resolution among various thicknesses of the counter substrate for (A) captured images and (B) horizontal profiles

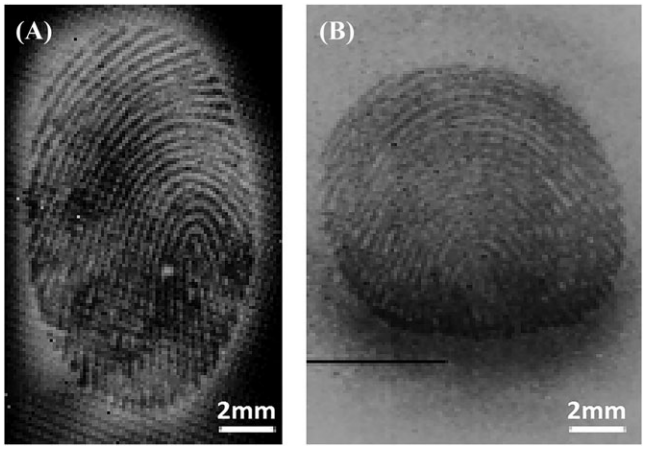

FIGURE 13 Captured image of fingerprint on (A) glass substrate and (B) flexible substrate

From Figure 12A, the black lines further become blurry and cannot be recognized at 0.7-mm counter substrate thickness; this tendency is also seen in Figure 12 B. At 0.2-mm counter substrate and without the light-shielding layer, although the black lines can be recognized in Figure 12A, the detected light intensity for the black lines increases and the contrast between the black lines and the background weakens as shown in Figure 12B. This trend is attributed to equalization of the intensity as the peripheral background region was simultaneously detected at wider image-capturing range of the OPD due to no usage of light-shielding layer, ie, a larger p, as earlier explained with Figure 11. At a counter substrate thickness of 0.2 mm and with the light-shielding layer, the black lines can be clearly observed in

FIGURE 14 Fingerprint image capturing on a flexible display

TABLE 2 Imaging conditions

	Emission Color for Imaging	Exposure Time, ms	Readout Time, ms
Figure 13A	Green	3.2	250
Figure 13B	Green	1.6	250

Figure 12A, and sharp peaks can be observed at intervals of 0.72 mm in Figure 12B. Since the width of the black lines being 0.12 mm is equal to the length of one size of a pixel, it can be understood that the image of the object was captured with the same resolution as the pixel density indicated in Table 1. For the succeeding section, we fabricated the prototype panels at $L = 0.2$ mm, in addition to the above-mentioned values of P, l, and s.

4.3 | Applications

Our prototype panels are expected to be useful in various applications, such as fingerprint identification.

Figure 13A presents an image of the fingerprint captured with a prototype display, which includes a glass substrate. Remarkably, the fingerprint was imaged with no known issues.

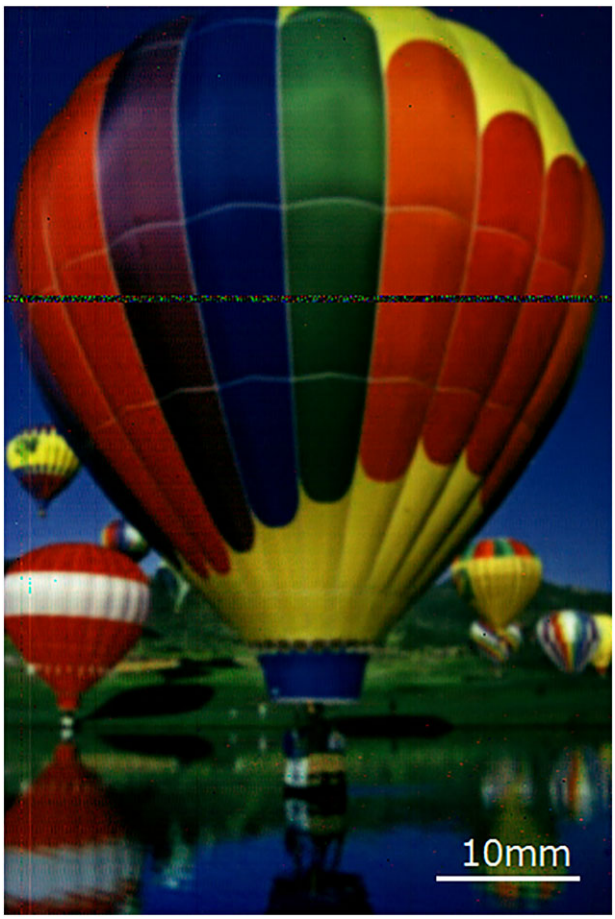

FIGURE 15 Image captured from a printed image

TABLE 3 Imaging conditions

Emission Color for Imaging	Exposure Time, ms	Readout Time, ms
Red	3.2	250
Green	3.2	250
Blue	3.2	250

For the flexible prototype display, an image of the fingerprint was captured at a bent portion, as shown in Figure 13B. The total thickness of the adhesive resin layer and the plastic film (L) was adjusted to 0.2 mm in the flexible panel. Figure 14 shows how the fingerprint image was captured at the bent-portion curvature radius of 10 mm, and Table 2 shows the imaging conditions. Although the image was blurry in the bent state as compared with the image captured in the flat state, it validated that imaging is possible even at the bent portion of the flexible display. This finding is significant, for example, in fingerprint identification at a curved portion of a side-roll display, as is recently employed in OLED-mounted smartphones.

This application can be stretched to a color scanner. Although sensor pixels corresponding to RGB colors are individually provided in a normal color image sensors, it is difficult to provide OPDs corresponding to those colors individually in our prototype display, in terms of the aperture ratio and the resolution. Our prototype display can capture a color image by sequentially making RGB OLEDs emit light by time division to obtain monochrome data for each of the RGB colors and then synthesizing the image data, as the material of the active layer employed in the incorporated OPD is capable of absorption in a wide visible light region. Figure 15 shows a captured color image. The same image displayed on the panel in Figure 6 was printed on a piece of glossy paper, and the printed image was captured while placed face-down (to the panel side) on the panel. Table 3 details the imaging conditions for this activity. The prototype panel employed a global shutter method, which enabled a color image to be obtained at 1 Hz. Furthermore, with the Pixel AI function, light emission with high luminance was achieved during image capturing.

5 | CONCLUSION

This study detailed the fabrication of the prototype OLED display incorporating the organic image sensor through side-by-side patterning. It validated the prototype's capability to perform imaging of a fingerprint and scanning

of an image over the entire display region. Therefore, its promising applications in flexible devices are expected.

ORCID

Taisuke Kamada https://orcid.org/0000-0002-0935-8610

REFERENCES

1. Maltoni D, Maio D, Jain AK, Prabhakar S. *Handbook of Fingerprint Recognition* 2nd ed.London: Springer-Verlag; 2009.
2. Bae S, Ling Y, Lin W, Zhu H. Optical fingerprint sensor based on a-Si:H TFT technology. SID Symposium Digest. 2018;49:1017–1020.
3. Kim JH, Lee JK, Chang YG, Moon BJ. Fingerprint scanner using a-Si: H TFT-array. SID Symposium Digest. 2000;31:353–355.
4. Halls JJM, Pichler K, Friend RH, Moratti SC, Holmes AB. Exiton diffusion and dissocitation in a poly(p-phenylenvinylene)/C60 heterojunction photovoltaic cell. Appl. Phys. Lett. 1996;68:3120–3122.
5. Shaheen SE, Brabec CJ, Sariciftci NS, Padinger F, Fromherz T, Hummelen JC. 2.5% efficient organic plastic cells. Appl. Phys. Lett. 2001;78:841–843.
6. Akkerman H, Peeters B, van Breemena AJ, et al. Printed organic photodetector arrays and their use in palmprint scanners. SID Symposium Digest. 2018;49:494–497.
7. Yamazaki S, Tsutsui T. *Physics and Technology of Crystalline Oxide Semiconductor CAAC-IGZO: Application to Displays*Chichester, UK: John Wiley; 2017.
8. Yuan CH, Lee CC, Liu CF, et al. Cathodic-controlled and near-infrared organic upconverter for local blood vessels mapping. Sci. Rep. 2016;6:32324.
9. Chiba T, Kumagai D, Udagawa K, Watanabe Y, Kido J. Dual mode OPV-OLED device with photovoltaic and light-emitting functionalities. Sci. Rep. 2018;8:11472.
10. Yamazaki S, Koyama J, Yamamoto Y, Okamoto K. Research, development, and application of crystalline oxide semiconductor. SID Symposium Digest. 2012;43:183–186.
11. Yamazaki S, Suzawa H, Inoue K, et al. Properties of crystalline In–Ga–Zn-oxide semiconductor and its transistor characteristics. Jpn. J. Appl. Phys. 2014;53:04ED18.
12. Kimizuka N, Yamazaki S. *Physics and Technology of Crystalline Oxide Semiconductor CAAC-IGZO: Fundamentals*Chichester, UK: John Wiley; 2017.
13. Yamazaki S, Hirohashi T, Takahashi M, et al. Back-channel-etched thin-film transistor using c-axis-aligned crystal In-Ga-Zn oxide. J Soc Inf Display. 2014;22(1):55–67.
14. Ito S, Takahashi E, Dairiki K, et al. Analysis of nanoscale crystalline structure of In-Ga-Zn-O thin film with nano beam electron diffraction. Proc. AM-FPD'13 Digest. 2013:151–154.
15. Yamazaki S, Shima Y, Hosaka Y, Okazaki K, Koezuka J. Achievement of a high-mobility FET with a cloud-aligned composite oxide semiconductor. Jpn. J. Appl. Phys. 2016;55:115504.
16. Kimizuka N, Mohri T. Spinel, $YbFe_2O_4$, and $Yb_2Fe_3O_7$ types of structures for compounds in the In_2O_3 and Sc_2O_3—A_2O_3—BO systems [A: Fe, Ga, or Al; B: Mg, Mn, Fe, Ni, Cu, or Zn] at temperatures over 1000°C. J. Solid State Chem. 1985;60:382–384.
17. Nakamura M, Kimizuka N, Mohri T. The phase relation in the In_2O_3 Ga_2ZnO_4 ZnO system at 1350°C. J. Solid State Chem. 1991;93:298–315.
18. Yamada Y, Matsubayashi D, Matsuda S. Single crystalline In-Ga-Zn oxide films grown from c-axis aligned crystalline materials and their transistor characteristics. Jpn. J. Appl. Phys. 2014;53:091102.
19. Nomura K, Ohta H, Takagi A, Kamiya T, Hirano M, Hosono H. Room-temperature fabrication of transparent flexible thin-film transistors using amorphous oxide semiconductors. Nature. 2004;432:488–492.
20. Kamiya T, Kimoto K, Ohashi N. Electron-beam-induced crystallization of amorphous In-Ga-Zn-O thin films fabricated by UHV sputtering. Proc. IDW'13 Digest. 2013:280–281.
21. Waseda Y, Sugiyama K, Kawamata T. Nanometer-sized crystalline clusters of IGZO films determined from the grazing incidence X-ray scattering and anomalous X-ray scattering data combined with reverse Monte Carlo simulations. Mater. Trans. 2018;59(11):1691–1700.
22. Kato K, Shionoiri Y, Sekine Y, et al. Evaluation of off-state current characteristics of transistor using oxide semiconductor material, indium–gallium–zinc oxide. Jpn. J. Appl. Phys. 2012;51:021201.
23. Aoki T, Ikeda M, Kozuma M, et al. Electronic global shutter CMOS image sensor using oxide semiconductor FET with extremely low off-state current. Proc. VLSI Technology Symp. 2011:174–175.
24. Amano S, Harada H, Akimoto K, et al. Low power LC display using In-Ga-Zn-oxide TFTs based on variable frame frequency. SID Symposium Digest. 2010;41:626–629.
25. Kataoka Y, Imai H, Nakata, Y et al. Development of IGZO-TFT and creation of new devices using IGZO-TFT. SID Symposium Digest. 2013;44:771–774.
26. Takahashi K, Kusunoki K, Watanabe K, et al. A novel touch-control method with partial scanning for LC, OLED, and hybrid displays using an oxide semiconductor. SID Symposium Digest. 2017;48:930–933.
27. Eguchi S, Nakamura D, Kusunoki K, et al. Strategy for developing an ultra-high-luminance AMOLED display. SID Symposium Digest. 2018;49:433–436.

AUTHOR BIOGRAPHIES

Taisuke Kamada received his BS and MS degrees in Physics from Tokyo University of Science, Japan, in 2013 and 2015, respectively. After graduation, he joined Semiconductor Energy Laboratory Co, Ltd and has been engaged in R&D of OLED displays.

Ryo Hatsumi received his BE and ME degrees in Material Science and Engineering from Yokohama National University, Japan, in 2008 and 2010, respectively. After graduation, he joined Semiconductor Energy Laboratory Co, Ltd and has been engaged in R&D of TFT-LCD.

Kazunori Watanabe received his ME degree in Graduate School of Information Science and Electrical Engineering from Kyushu University, Japan, in 2008. After graduation, he joined Semiconductor Energy Laboratory Co, Ltd and has been engaged in a circuit design of LCD/OLED displays and touch panels.

Susumu Kawashima received his BE and ME degrees in Physics from Tokyo University of Science, Japan, in 2008 and 2010, respectively. After graduation, he joined Semiconductor Energy Laboratory Co, Ltd. Since then, he has been engaged in the circuit design of OLED display.

Masahiro Katayama graduated from Japan Aviation Technical College, Japan, in 1999. He joined Semiconductor Energy Laboratory Co, Ltd in 1999. Since then, he has been working on the manufacturing process and the development of OS-FET.

Hiroki Adachi graduated from Japan Aviation Technical College, Japan, in 1990. After graduation, he joined Semiconductor Energy Laboratory Co, Ltd and has been engaged in the manufacturing process. And since 2008, he has been working on the development of flexible process technology.

Tetsuji Ishitani received his BE and ME degrees from Tokyo University of Science, Japan, in 1998 and 2000, respectively. After graduation, he joined Semiconductor Energy Laboratory Co, Ltd and has been engaged in R&D of TFT-LCD.

Koji Kusunoki received his BE and ME degrees in Pure and Applied Physics from Waseda University, Japan, in 2006 and 2008, respectively. After graduation, he joined Semiconductor Energy Laboratory Co, Ltd and has been engaged in designing flat panel displays like LCDs and OLED displays.

Daisuke Kubota received his BS and MS degree in Physics from Tokyo University of Science, Japan, in 2001 and 2003, respectively. After graduation, he joined Semiconductor Energy Laboratory Co, Ltd and has been engaged in R&D of TFT-LCD.

Shunpei Yamazaki received his PhD, ME, BE, and honorary degrees from Doshisha University, Japan, in 1971, 1967, 1965, and 2011 respectively. He is the founder and president of Semiconductor Energy Laboratory Co, Ltd. He was awarded with Medal with Purple Ribbon by the Japanese Prime.

How to cite this article: Kamada T, Hatsumi R, Watanabe K, et al. OLED display incorporating organic photodiodes for fingerprint imaging. *J Soc Inf Display*. 2019;1–11. https://doi.org/10.1002/jsid.786